Analyst

PAPER

View Article Online
View Journal | View Issue

Cite this: *Analyst*, 2019, **144**, 2942

Label-free density-based detection of adipocytes of bone marrow origin using magnetic levitation†

Oyku Sarigil, ‡[a] Muge Anil-Inevi, ‡[a] Esra Yilmaz, [a] Gulistan Mese, [b] H. Cumhur Tekin [a] and Engin Ozcivici *[a]

Received 26th December 2018,
Accepted 10th March 2019

DOI: 10.1039/c8an02503g

rsc.li/analyst

Adipocyte hypertrophy and hyperplasia are important parameters in describing abnormalities in adipogenesis that are concomitant to diseases such as obesity, diabetes, anorexia nervosa and osteoporosis. Therefore, technical developments in the detection of adipocytes become an important driving factor in adipogenesis research. Current techniques such as optical microscopy and flow cytometry are available in detection and examination of adipocytes, driving cell- and molecular-based research of adipogenesis. Even though microscopy techniques are common and straightforward, they are restricted in terms of manipulation and separation of the cells. Flow cytometry is an alternative, but mature adipocytes are fragile and cannot withstand the flow process. Other separation methods usually require labeling of the cells or usage of microfluidic platforms that utilize fluids with different densities. Magnetic levitation is a novel label-free technology with the principle of movement of cells towards the lower magnetic field in a paramagnetic medium depending on their individual densities. In this study, we used a magnetic levitation device for density-based single cell detection of differentiated adipogenic cells in heterogeneous populations. Results showed that the magnetic levitation platform was sensitive to changes in the lipid content of mesenchymal stem cells committed to adipogenesis and it could be successfully used to detect the adipogenic differentiation of the cells.

Introduction

Adipose tissue, once considered only as a tissue type that provides mechanical support, thermal insulation and energy storage, is now known to support crucial endocrine and immune functions in various tissues.[1–4] For example, abnormal adipogenesis in bone marrow can be observed in several diseases such as obesity, diabetes, anorexia nervosa and osteoporosis.[5–11] Marrow adipocytes are derived from mesenchymal stem cells (MSCs), which also have the capability to differentiate into osteoblasts.[12–15] Once a marrow adipocyte is formed, it can interfere with cellular differentiation, bone remodeling and hematopoiesis.[6,11,16,17] There is a negative relationship between bone marrow adipocytes and bone density,[18,19] and the disturbed balance between adipogenesis and osteoblastogenesis may inhibit bone reformation.[20–25] Similarly, skeletal aging also shifts the balance to increased adipogenesis, leading to the yellow bone marrow phenotype.[10,18,26,27] Marrow adipogenesis can further be linked to changes in important immune and endocrine system functions.[28–31]

Complex functions of adipocytes with their strong association to the epidemiology of obesity and obesity-related diseases have remarkably increased the interest in morphology and physiology of adipocytes.[32] In this context, it has become critical to detect and identify adipocytes for hypertrophy (increasing cell size) and hyperplasia (increasing cell number) and thus to examine the underlying mechanisms of the formation and development of the adipose tissue in healthy and abnormal tissues.[33,34] Adipocyte detection on the cellular level relies on the formation of intracellular lipid droplets and an increase in cell volume.[35–37] Optical microscopy is commonly used to visualize adipocyte differentiation by staining the cells with lipophilic dyes such as Oil Red O, Nile Red and Sudan Red.[38–40] Although optical microscopy is useful for the detection and examination of the monolayer lipid-accumulated cells, produced results mainly lead to a qualitative assessment. Adipogenic differentiation can also be observed through molecular markers of adipogenesis such as P107, PPARγ, C/EBPα and aP2;[24,41–43] however, these techniques are time-consuming and labor-intensive and do not allow the recovery of the cells for further studies. Advanced techniques, such as flow cytometry, can be used to detect differentiated adipocytes.[36] However,

[a]*Department of Bioengineering, Izmir Institute of Technology, Urla, Izmir, Turkey. E-mail: enginozcivici@iyte.edu.tr; Fax: +90 232 750 7603; Tel: +90 232 750 7385*
[b]*Department of Molecular Biology and Genetics, Izmir Institute of Technology, Urla, Izmir, Turkey*

†Electronic supplementary information (ESI) available. See DOI: 10.1039/c8an02503g

‡Equal contribution.

nozzles in these systems limit the application to pre-adipocytes, as mature adipocytes are fragile and cannot withstand the flow.[44–46] Alternative cell separation platforms are available based on fluorescent or magnetic markers[47–49] or utilization of complex microfluidic platforms that use fluid interfaces where cells are stratified on different fluids based on their densities.[50] Sensors that can track changes in electric cell–substrate or using Coherent anti-Stokes Raman scattering (CARS) imaging can also be used as label-free methods;[51–53] however, these techniques are relatively expensive, require complex instrumentation and cannot perform single cell detection.

Cell density can be utilized as an indicator of the cell state such as apoptosis, disease state and cell cycle.[54–57] Changes in cell density are also observed during cellular differentiation.[58] The conventional method to determine cell density is *via* density gradient centrifugation.[59,60] Even though this technique is relatively simple and cost-effective, it may cause cell damage due to high centrifugal forces with long operation time needed to obtain the density gradient contrary to the acceptable operation effect of the process on the cells to collect them from medium.[60,61] More importantly, this method can only yield the average density of the target cell population and cannot discriminate small differences in cell densities.[50,62] Density measurements based on a single cell are possible through microfluidic technology, such as the suspended microchannel resonator (SMR) system[58,59] and optically induced electrokinetics (OEK) platform.[63] Although the SMR system is very precise in measuring single cell density, it is time-consuming and compatible liquids with different densities need to be selected specifically to the particular application.[64] The OEK platform, on the other hand, has a complex design with optical elements and virtual electrode setups. An alternative methodology for single cell density measurements is the magnetic levitation technology that allows the real-time, label-free separation of cell populations with the principle of movement of the cells towards the lower magnetic field in a paramagnetic medium based on their density.[62,65–67] When diamagnetic substances such as cells are placed in a magnetic field, they acquire a net magnetic moment in the opposite direction to the magnetic field and they are repelled to the weaker magnetic field region. This repulsive force can be amplified *via* paramagnetic agents that alter the magnetic susceptibility of the medium to acquire levitation.[68,69] In the magnetic manipulation of diamagnetic objects, the distribution of the magnetic field can be controlled by varying the positions of the magnets with reference to each other, leading to the manipulation of the net magnetic force on the target objects.[70] The magnetic levitation system has been previously applied with different shapes and configurations of magnets to improve accuracy and throughput in the detection of object/cell densities.[71–74] Though the magnetic levitation system is applicable to the single cell density-based detection of cancer, blood cell subtypes, bacteria, and yeast cells, its applicability in the detection of adipogenesis was not tested before.

In this study, a quantitative method was demonstrated to detect the changes in the single cell density of lipid-accumulated bone marrow cells during adipogenic differentiation by using the magnetic levitation principle. We showed that the magnetic levitation platform was sensitive to changes in the lipid content of mesenchymal stem cells committing to adipogenesis, and it could be successfully used to detect the adipogenic differentiation of the cells. We believe this quantitative, cost-effective and label-free microfluidic system serves as a potential method to be applied in future adipocyte and lipid research.

Results

Microfluidic setup for magnetic levitation

In this study, we used a custom-designed microfluidic platform that is composed of a holder, two opposing neodymium magnets, a capillary channel that can hold cells in a paramagnetic medium, and two parallel mirrors to visualize cell levitation (Fig. 1A). The platform can generate magnetic forces (F_{mag}) that can balance the buoyancy force (F_b) which is the combination of gravity and buoyancy force vectors (Fig. 1B). Based on FEM solution of the magnetic induction (B) in the gravitational direction between the magnets (Fig. 1C), we identified a potential range of single cell densities that our platform can resolve based on the equation:[66] $\Delta\rho = (B\cdot\nabla)B(\Delta\chi/(\mu_0\cdot g))$, where $\Delta\rho$ is the density difference between the paramagnetic medium ($\rho_{solution}$) and the cell (ρ_{cell}), $\Delta\chi$ is the magnetic susceptibility difference between the paramagnetic medium and the cell, μ_0 is the permeability of free space, and g is the gravitational acceleration, for different concentrations of gadolinium (Gd^{3+}) in media (Fig. 1D). According to the results, the measurable cell density (ρ_{cell}) interval of the magnetic levitation system is 0.956–1.055 g mL^{-1} at 10 mM, 0.882–1.130 g mL^{-1} at 25 mM, 0.760–1.256 g mL^{-1} at 50 mM, 0.637–1.381 g mL^{-1} at 75 mM and 0.515–1.507 g mL^{-1} at 100 mM Gd^{3+} concentration. Even though 10 mM Gd^{3+} indicated the best resolution value at 0.0000591 (g mL^{-1}) per micrometer distance (Fig. 1E), based on the limited range of densities at 10 mM we continued the study using concentrations between 25 and 100 mM of Gd^{3+}.

Calibration of the magnetic levitation system with polymeric beads

Prior to levitation of cells, the microfluidic device was calibrated for the density-based detection of adipogenesis *via* determining the levitation heights of polymeric beads with known densities (1 g mL^{-1}, 1.02 g mL^{-1} and 1.09 g mL^{-1}) in the culture medium containing paramagnetic gadolinium (Gd^{3+}) at 25 mM, 50 mM and 100 mM concentrations (Fig. 2A). Increased bead densities and decreased Gd^{3+} concentrations lead to lower levitation heights, which was measured as the average bead distance from the top surface of the bottom magnet. Levitation heights of the beads with 1.09 g mL^{-1} were 37.15%, 22.86% and 13.76% lower than those of the beads with 1 g mL^{-1} in the medium containing 25 mM, 50 mM and 100 mM Gd^{3+} (all $p < 0.05$), respectively (ESI Fig. S1†).

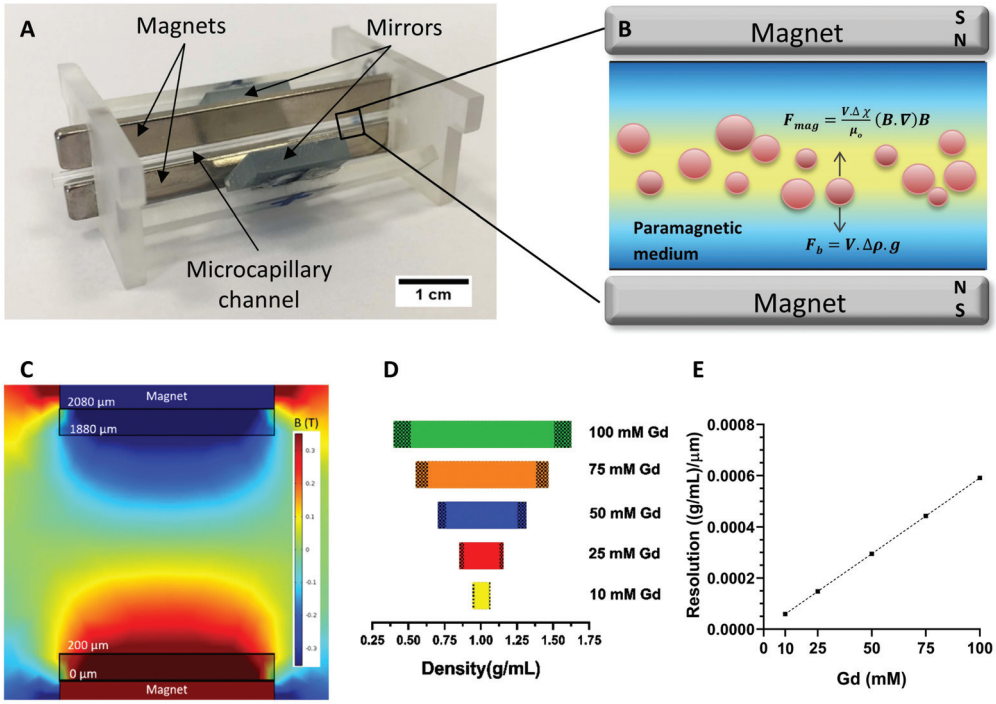

Fig. 1 The magnetic levitation setup and working principle. (A) Structure of the magnetic levitation device composed of two neodymium magnets, a microcapillary channel and two mirrors placed at 45°. (B) Forces acting on cells at the equilibrium position in the device, where F_{mag}: magnetic force, F_b: buoyancy force, V: cell volume, $\Delta\chi$: magnetic susceptibility difference between the paramagnetic medium and the cell, μ_0: permeability of free space, B: magnetic induction, $\Delta\rho$: density difference between the paramagnetic medium and the cell, g: gravitational acceleration. (C) Cross-sectional representation of the magnetic induction between magnets in the direction of gravitational acceleration. Shaded areas are not accessible because of capillary wall thickness. (D) The range of single cell density values that can be measured with the microfluidic setup with respect to Gd^{3+} concentrations used based on the computational model. (E) Density resolution of the levitation system with respect to Gd^{3+} concentrations based on the computational model.

Furthermore, an increased Gd^{3+} concentration decreased the difference in levitation heights between different densities of polymeric beads defining the working span of the microfluidic device. The difference between the levitation heights of beads (range) with densities of 1.09 g mL^{-1} and 1 g mL^{-1} was found as 425 µm, 261 µm and 156 µm (Fig. 2A; blue arrows), when levitation was performed with 25 mM, 50 mM and 100 mM Gd^{3+}, respectively. Similarly, the increased Gd^{3+} concentration decreased the range between beads with densities of 1.09 g mL^{-1} and 1.02 g mL^{-1} from 346 µm to 203 µm and to 116 µm (Fig. 2A; red arrows). The inverse relation of the levitation height and bead density values showed a strong correlation ($R^2 > 0.99$) for different Gd^{3+} concentrations (Fig. 2B) with the linear fits $\rho = -0.000209001 \times h + 1.240573$ for 25 mM Gd^{3+}; $\rho = -0.000344456 \times h + 1.393534$ for 50 mM Gd^{3+}; and $\rho = -0.000583928 \times h + 1.659352$ for 100 mM Gd^{3+}, where ρ corresponds to the density (g mL^{-1}) and h corresponds to the levitation height (µm).

Detection of the adipogenic cells with the microfluidic platform

D1 ORL UVA bone marrow mesenchymal stem cells were chosen as an initial experimental model for this study. D1 ORL UVA cells were first treated with an adipogenic induction medium for 15 days along with growth media controls (ESI Fig. S2†). The cells reached confluency in both groups at the end of the first week. In contrast to the cells in the growth medium, a fraction of cells treated with the adipogenic induction started to accumulate lipid droplets at the end of the first week, and they continued to accumulate lipid droplets leading to hypertrophy. After 15 days of culture in the induction medium, lipid accumulated cells were levitated in the microfluidic device at 25 mM, 50 mM and 100 mM Gd^{3+} concentrations (Fig. 3). In accordance with data obtained from polymeric beads, 100 mM Gd^{3+} resulted in a narrow band of 225 µm between the average levitation height of the high-density bulk cell population and the levitation height of the adipogenic cells with the lowest density. Decreasing the Gd^{3+} concentration increased this distance to 273 µm for 50 mM and 377 µm for 25 mM. Since the sensitivity of the levitation system to density changes in particles/cells increased as Gd^{3+} concentration decreased, we continued further experiments with 25 mM Gd^{3+} concentration. An *in situ* live/dead staining revealed that all cells, including cells that were large-sized and levitated at higher levels, appeared healthy (ESI Fig. S3†).

Determination of density profiles of adipogenic cells

In order to assess the effect of adipogenic culture on levitation height, D1 ORL UVA cells were cultured with the growth or the adipogenic induction medium in plates up to 15 days. The cells were then levitated at the 1st, 5th, 8th, 12th and 15th

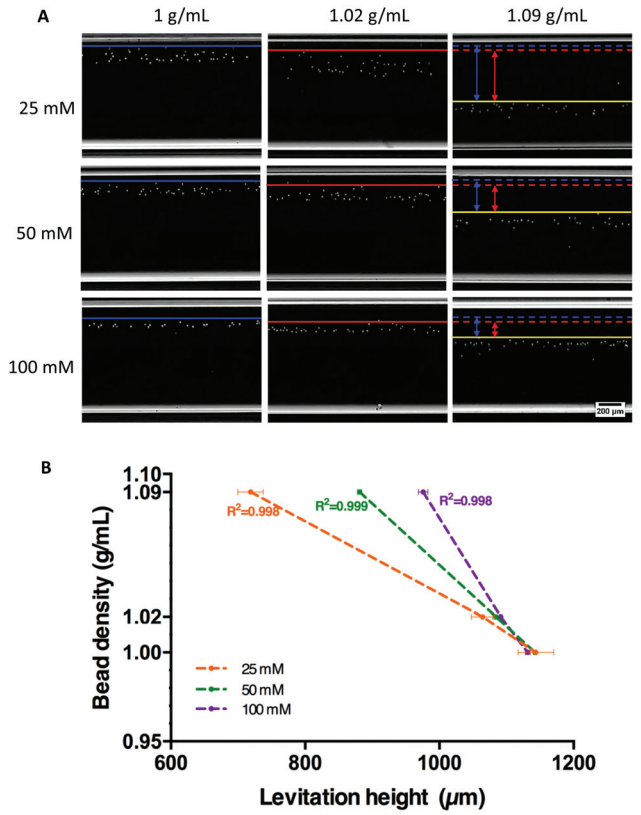

Fig. 2 Calibration of the magnetic levitation system by using polymeric beads with known densities. (A) Images of the magnetically levitated beads with different densities (1 g mL^{-1}, 1.02 g mL^{-1} and 1.09 g mL^{-1}) in the culture medium containing 25 mM, 50 mM or 100 mM Gd^{3+} solution. The blue line presents the uppermost level of the levitation heights of the beads with 1 g mL^{-1} density, the red line with 1.02 g mL^{-1}, and the yellow line with 1.09 g mL^{-1}. Blue and red arrows show the difference of levitation heights of the beads between densities of 1.09 g mL^{-1}, and 1 and 1.02 g mL^{-1}. Scale bar: 200 μm. (B) Correlation between the levitation height and the density of beads. For each Gd^{3+} concentration (25, 50 and 100 mM), a linear equation was obtained with determined levitation heights of beads (R^2 = 0.998, R^2 = 0.999 and R^2 = 0.998, respectively). Data are represented as mean ± SD.

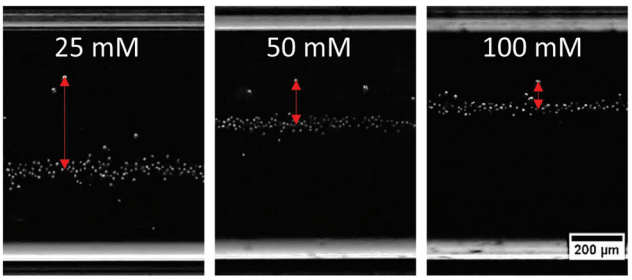

Fig. 3 Optimization of the paramagnetic medium concentration in the detection system. Magnetic levitation images of D1 ORL UVA cells cultured in the adipogenic differentiation medium at the 15th day using 25, 50 and 100 mM Gd^{+3} concentrations. Red arrows indicate the height difference between the average levitation height of general cell population and cells with the lowest density, indicating the range of density-based distribution. Scale bar: 200 μm.

days of culture in the levitation system using 25 mM Gd^{3+} concentration, and changes in the density of the cells depending on the treatment time were analyzed (Fig. 4). At the first day of culture, control and adipogenic cells resided in similar levitation heights, while at day 15, a fraction of cells subjected to adipogenic induction was positioned at higher levitation heights (Fig. 4A). Cells in the growth medium at day 1 were located at 761 ± 49 μm from the bottom magnet corresponding to the density of 1.081 ± 0.010 g mL^{-1} according to the previously obtained equation for 25 mM Gd^{3+} concentration (Fig. 4B). At day 15, control cells similarly resided at 740 ± 31 μm corresponding to the density of 1.086 ± 0.005 g mL^{-1}. Cells in the adipogenic induction medium had a similar average density compared to the control cells at both day 1 (p = 0.96) and day 15 (p = 0.33) (Fig. 4C). Skewness of the cell density distribution between groups was also similar between groups (p = 0.94) at day 1 (Fig. 4D). We further assessed density in the lower density fractions of cells, and at day 1, average densities of cells in the lowest 5th percentile for cells cultured in growth and adipogenic induction media were similar (p = 0.71) (Fig. 4E). At day 15, however, the average density of the cells residing in the lowest 5th percentile of density was 1.79% lower for the adipogenic cells (p = 0.03) than for the controls, and 1.79% of the adipogenic population had density values smaller compared to the lowest density recorded (1.052 g mL^{-1}) for the control cells (Fig. 4D). Furthermore, the skewness of the density distribution for the cells cultured in the growth and adipogenic media was 0.99 ± 0.6 and −2.3 ± 0.6 (p = 0.02), respectively (Fig. 4E). Physical changes in the D1 ORL UVA cells during adipogenesis not only were limited to a reduction in the density but also affected the cell size. The cells that had a lower density than the average density of the growth control cells (1.084 g mL^{-1}) at day 1 were analyzed for a measure of change in size during adipogenesis (Fig. 5A and B). At the first day, there was no significant difference between quiescent and adipogenic induced cells that had 51 ± 18 μm^2 and 36 ± 20 μm^2 cell size on average, respectively (p = 0.06). The cells in adipogenic induction had a slight but significant increase from 36 ± 19 μm^2 at day 1 to 45 ± 28 μm^2 at day 15 (p = 0.05). Furthermore, there was a significant correlation between the size and density of the cells (R^2 = 0.29) in contrast to undifferentiated cells (R^2 = 0.01) after 15 days of culture (Fig. 5C and D).

Since the lipid accumulation process of the D1 ORL UVA cells was relatively slow and affected only a fraction of the population, we extended our study to adipogenesis in 7F2 cells, a bone marrow cell line that can accumulate a large amount of lipids in a relatively short time. The cells were cultured in a similar growth medium or adipogenic differentiation medium for 10 days (ESI Fig. S4†) and levitated at the 1st, 5th and 10th days of culture with 25 mM Gd^{3+} (Fig. 6). The cell density of the entire adipogenic cohort at the 1st day of culture was 1.079 ± 0.005 g mL^{-1} and decreased 1.76% (p < 0.001) to 1.060 ± 0.029 g mL^{-1} after 10 days in the adipogenic culture. Furthermore, average densities of the cells in the 5th percentile for 7F2 cells cultured in the adipogenic induction

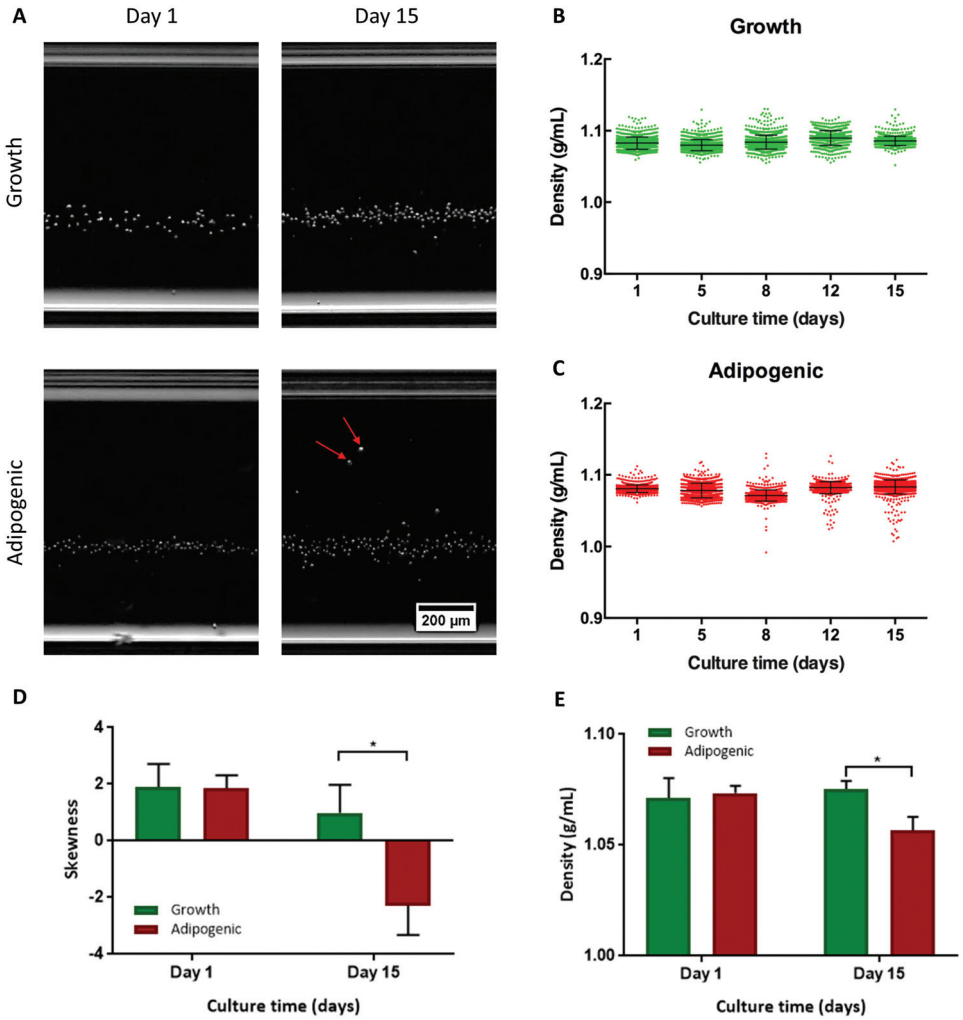

Fig. 4 Levitation and density profiles of D1 ORL UVA cells using 25 mM Gd^{3+}. (A) Levitation images of quiescent and adipogenic D1 ORL UVA cells at the 1st and 15th days. Arrows indicate differentiated cells with lower densities. Scale bar: 200 μm. (B, C) Scatter plots of densities of quiescent and adipogenic differentiated cells at the 1st, 5th, 8th, 12th and 15th days. Data are represented as scattered with an inset of mean ± SD. (D) Skewness of density values of control and adipogenic populations at the 1st and 15th days. (E) Average density values of the lowest 5th percentile pertaining to control and adipogenic populations. Data are represented as mean ± SD. *: $p < 0.05$; **: $p < 0.01$; ***: $p < 0.001$.

medium for 10 days were observed as 1.003 ± 0.002 g mL^{-1} with a minimum density of 0.989 g mL^{-1}, and 37% of the adipogenic cell population had a lower density compared to the lowest density observed in the cells that were kept in the growth medium for 10 days.

Detection of adipogenic differentiated cells mixed with stem cell population

In order to test whether the magnetic levitation system can be used in the detection of adipogenic cells in a mixed cell population, quiescent D1 ORL UVA cells (tracked with the green fluorescent dye) and adipogenic-differentiated 7F2 cells (tracked with the red fluorescent dye) were mixed at 1%, 5%, 10%, 25%, 50% (percentage of adipogenic 7F2 in the mix) ratios and levitated with a medium containing 25 mM Gd^{3+} (Fig. 7A, ESI Fig. S5†). Results showed that increasing the culture period resulted in an enhanced difference between the relative densities of the differentiated (7F2) and quiescent (D1) groups (Fig. 7B). For the group in which the quiescent cells and adipogenic cells were mixed at 50%, the average relative density of the cells obtained from the 1st day of culture was similar ($p = 0.45$), while 25.7% ($p < 0.001$) difference was recorded between the two cell groups at day 10. Similar trends were observed for other cell ratios. Even when the proportion of the adipogenic cells in the quiescent cell population was reduced to 1%, low-density 7F2 cells were distinctly observed in the detection system. To show that the differences observed in the levitation height were based on the differences in the densities and not the cell type, we levitated undifferentiated D1 ORL UVA and undifferentiated 7F2 cells (mixing ratio: 50%) at the 1st, 5th and 10th days of culture as a control group (ESI Fig. S6†), showing the cells had similar density values ($p > 0.05$) at all time points. Manual counting of the 7F2 cells (red) in the heterogeneous mix resulted in the determination of

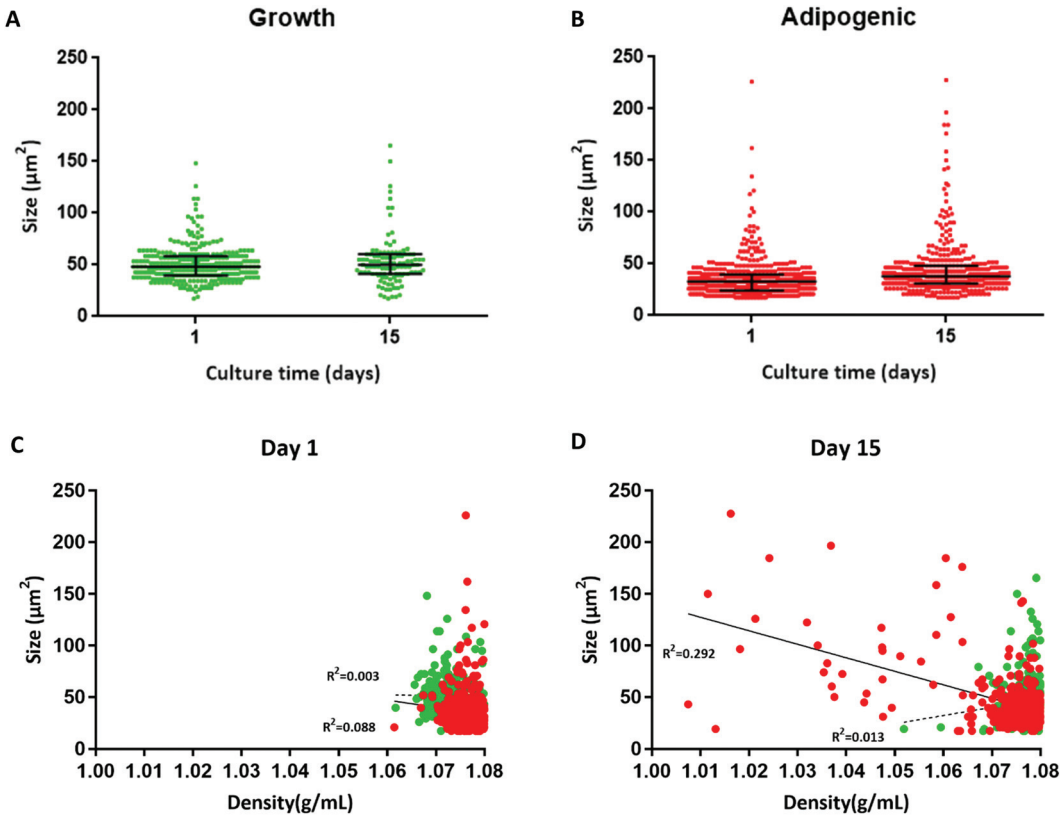

Fig. 5 Alterations in cell size (area, μm^2) during adipogenesis. (A, B) Size of quiescent and differentiated cells with density below 1.08 g mL^{-1} (average density of control cells) on day 1 and day 15 of culture. Data are represented as scattered with an inset of mean ± SD. (C, D) The relationship between size (area, μm^2) and density (g mL^{-1}) of D1 ORL UVA cells cultured within the growth and adipogenic media for day 1 and day 15 of culture. Scatter plot represents the relationship between density and size of differentiated and quiescent cells with density values <1.08 g mL^{-1}. Dashed and solid lines indicate linear regression for quiescent and differentiated cells, respectively.

observed adipogenic cell fractions in different mixes. Compared to expected 7F2 fractions, observed values were mostly similar ($p > 0.05$) as determined by the chi-square test (Fig. 7C). This similarity was more prominent in the 7F2 cells that originate from the 5th and 10th days of adipogenic culture, where cells were committed to adipogenesis (ESI Fig. S4†). Finally, we categorized cells assumption-free from light field images with respect to the levitation height and determined their lineages post stratification (Fig. 8). Capillary was separated into 3 density zones: zone I for cells with density below 1.02 g mL^{-1} (above the yellow line), zone II for >1.02 g mL^{-1} and <1.06 g mL^{-1} (between the blue and yellow lines), and zone III for >1.06 g mL^{-1} (below the blue line). According to the results at day 10, zones II and III were populated with undifferentiated cells, while zone I was exclusive to adipogenic 7F2 cells, showing that the system was highly selective for lipid accumulated cells.

Discussion

In this study, we tested a novel method to detect the adipogenic differentiation of bone marrow stem cells based on cell density by a magnetic levitation device. In summary, we firstly calibrated the detection system by using polymer beads with different densities to determine the correlation between levitation heights of particles and their density values depending on the concentration of the gadolinium contrast agent. Linear equations provided by the relationship between levitation heights and density values were used to measure the single cell density. Secondly, we aimed to determine the optimum gadolinium concentration that should be used to perform density-based detection with D1 ORL UVA bone marrow stem cells, as a model. Eventually, 25 mM concentration was chosen for the following experiments due to its high ability to distinguish adipogenesis-induced cells. Thirdly, the adipogenic cells in the stem cell population were successfully distinguished using the selected concentration in a heterogeneous population by the magnetic levitation technology.

The magnetic levitation system has been previously reported as a detection/characterization method for cancer cells in a population containing different blood cell types and as a drug testing system on prokaryotic cells.[62] In this system, blood cells (*i.e.*, red and white blood cells) were located at lower levitation heights with higher densities, and different types of cancer cells such as breast adenocarcinoma

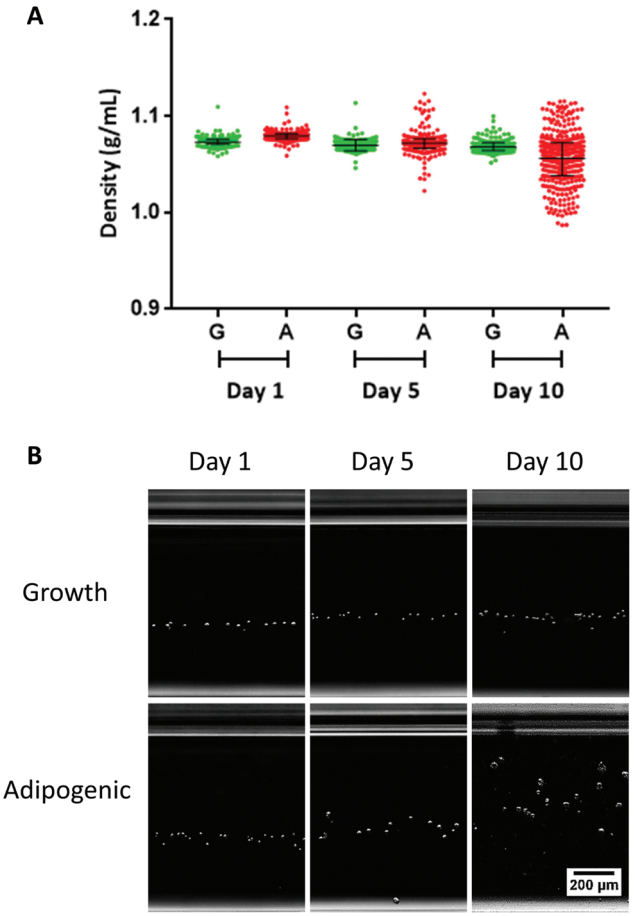

Fig. 6 Levitation of 7F2 cells in the magnetic levitation system. (A) Density dot plots of differentiated and undifferentiated cells at the 1st, 5th and 10th days of culture. Data are represented as scattered with an inset of mean ± SD. (B) Magnetic levitation (25 mM Gd^{3+}) images of the cells cultured in the growth and adipogenic culture media over 10 days. Scale bar: 200 μm.

(MDA-MB-231), esophageal adenocarcinoma (JHEsoAD1), colorectal adenocarcinoma (HT29) were positioned at higher levels as a result of their lower density values. On the other hand, the effect of the antibiotic treatment, known to cause cellular composition changes of bacterial cells, on the density of cells was shown in real time by the levitation system.[62,75] Here, we aimed to adapt the system to detect adipocytes by using the separation function of the principle depending on the density. In conclusion, the levitation system was successfully performed for the detection of adipogenic differentiated stem cells. The density of D1 ORL UVA stem cells and 7F2 osteoblast cells (>1.07 g mL^{-1}) is strongly consistent with the density of previously reported bone marrow-derived stem cells.[76,77] On the other hand, adipogenic cells were found to be less dense (down to 0.989 g mL^{-1}) than all these cell types, regardless of the origin of adipocytes. These results show that the magnetic levitation system has potential to distinguish different cell populations in the bone marrow. Even considering the suitability of this system for cell culture,[67] it is also promising that these cell types can be levitated and cultured at different levels in a single culture chamber and the interactions between these cells can be examined at the cellular and molecular levels.

The density range of the adipose tissue is determined as 0.925 and 0.970 g mL^{-1};[78] however, density values of adipocytes at the single cell level are not yet available in the literature. However, some density measurement techniques for single cells can be used to measure the density of adipocytes, such as OEK platform, or SMR. Contrary to these methods that measure single cell density by the help of cell mass and volume analyzed with complex and expensive instrumentations, our system offers a rapid and cost-effective way to measure densities by using a specific equation *via* the magnetic levitation system.[58,59,79] Adipocytes can be extremely large and fragile, restricting the applicability of flow cytometry for detection and sorting. Our system not only presents a label-free, real-time monitoring of the cells but also does not carry out any mechanical manipulation while flow cytometry uses flow pressure up to 10 psi.[45] Furthermore, adipocyte phenotype can be highly variable based on age,[80] gender[81] and body mass index,[82] where our system may provide a potential alternative with theoretical limits of resolution as low as 1×10^{-4} (g mL^{-1}) per micrometer distance. Other microfluidic systems for density measurement such as SMR require multiphase media consisting of two or more liquids with different densities.[50,55,58] The magnetic levitation technique does not need multiple phases with different liquids and thus offer ease of application. In addition, unlike other methods that allow analysis at the single cell level (*i.e.*, OEK microfluidic platform), the magnetic levitation platform provides density measurement of cells in great quantities at the same time.[63] Another advantage of this principle is that it allows label-free detection and it is possible to adapt the system to separate cells without modifications on them for the following studies.

We achieved density measurements of adipogenic cells, and findings revealed that lipid accumulation caused cells to position at higher levels than undifferentiated cells. This is an expected result since lipid droplets store neutral lipids in adipocytes that are formed primarily by triacylglycerols with a density below 1 g mL^{-1} (ref. 83 and 84), and these altered cytosol states reduce the single cell density to adipocytes compared to other cells. Previous studies demonstrated that adipocytes show heterogeneity in lipid droplet accumulation and morphology in response to the inducing agents, and the underlying mechanisms of this phenotypic heterogeneity are poorly known.[85–87] Therefore, it was thought that differences in levitation heights of adipocytes could be caused by either a difference in state and/or the number of accumulated lipid droplets of differentiated cells. Regardless, our detection system has potential to become an informative method related to lipid accumulation and cell state in contrast to current methods such as optical microscopy. Additionally, determination of adipocyte size is important for adipogenesis and

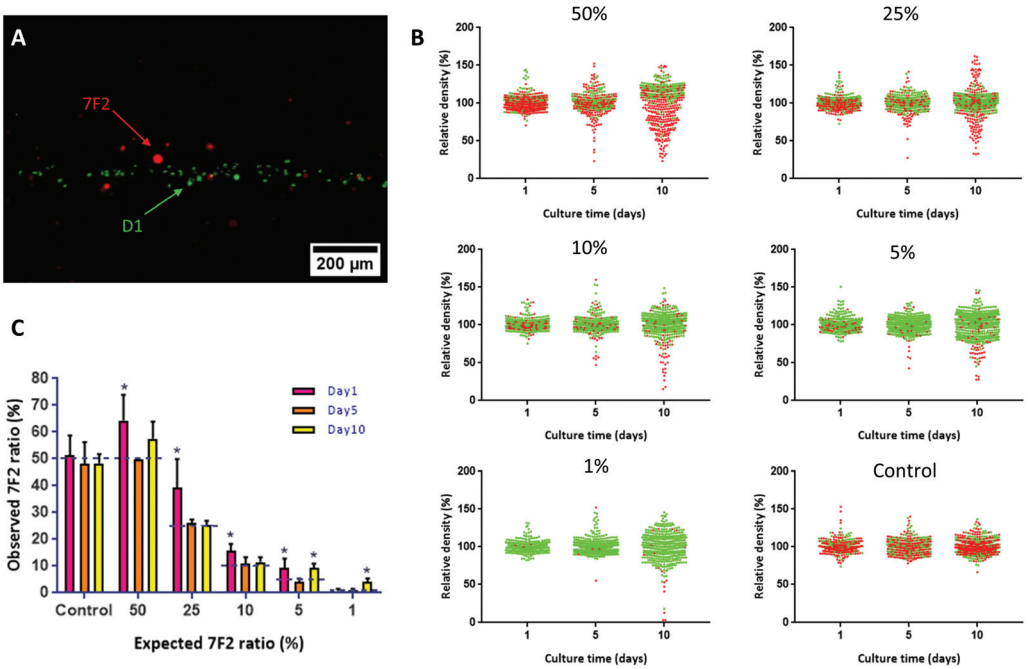

Fig. 7 Detection of adipogenic cells in a heterogeneous cell population. (A) A representative image of levitated quiescent D1 cells (green) and adipogenic differentiated 7F2 cells (red). Scale bar: 200 μm. (B) Scatter plot for the relative density (%) of adipogenic differentiated 7F2 cells and quiescent D1 ORL UVA cells, cultured for 1, 5 and 10 days and mixed at different ratios of 7F2 cells (50%, 25%, 10%, 5% and 1%) and undifferentiated 7F2 cells (red) and quiescent D1 ORL UVA cells with a ratio of 50%, as control, for magnetic levitation (25 mM Gd^{3+}). (C) Observed ratios of adipogenic differentiated 7F2 cells in these heterogeneous populations with the magnetic levitation based detection system. Control group indicates undifferentiated 7F2 cells mixed with quiescent D1 ORL UVA cells with a ratio of 50%. The chi-square test was performed for statistical analysis. Scale bar: 200 μm. Statistical significance was defined as *: $p < 0.05$; **: $p < 0.01$; ***: $p < 0.001$.

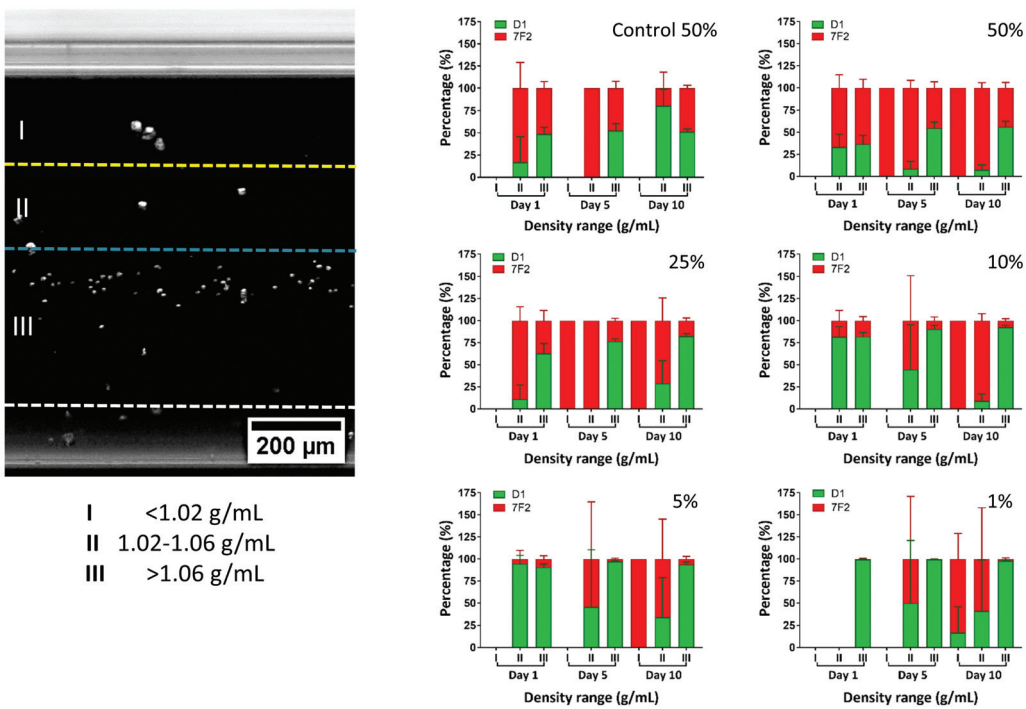

Fig. 8 Assumption-free categorization of 7F2 and D1 ORL UVA cells based on their density (zone I: for <1.02 g mL^{-1}, zone II: for >1.02 g mL^{-1} and <1.06 g mL^{-1}, and zone III: for >1.06 g mL^{-1}). Stacked bar graphs indicate the ratio of the corresponding cell type in the zone, red: 7F2, green: D1 ORL UVA.

metabolic studies since the increase in cell size of adipocytes is one of the parameters of adipogenesis and also adipocyte size influences the cellular metabolism rate.[33,34,88] Some metabolic functions such as secretion of cytokines by adipocytes are believed to be related to adipocyte size, and size changes are relatable to disorders such as obesity, insulin resistance and type 2 diabetes.[89,90] Previous techniques for determination of the size of adipocytes are generally time-consuming and terminal that rely on cell fixation and then monitoring cell images obtained with a camera.[88,91] In contrast to these systems, our system provides simultaneous monitoring of the relationship between cell density and cell size as evidenced by the inverse correlation between size and density in adipocytes during the lipid accumulation process.

Besides the targeted cellular changes to be tested (*i.e.*, differentiation), we also noticed that the culture conditions might affect the density of the cells. In this study, we tried longer term culturing of D1 ORL UVA cells to 3 weeks to increase the adipogenic fraction. But this resulted in non-homogenous distribution of both control and adipogenic cells in the levitation system, potentially from reduced cellular health and confined cell sizes (data not shown). Also, it was observed that while some cells showed an expected decrease in density, some part of the population showed an unexpected increase during adipogenic induction. Although the complicated mechanism of cell density regulation has not been fully explained yet, previous studies have shown that some factors such as osmolality and cell cycle have effects on cell density.[92,93] Another issue to be considered in the determination of density using the magnetic levitation system is the magnetic susceptibility of the paramagnetic medium. Although 25 mM Gd^{3+} is appropriate to distinguish the cell types, stem cells and adipocytes used here, this value may be required to be customized for high-resolution detection in cell combinations with the different range of density.

In conclusion, our method provides a label-free, real-time detection system for adipogenic differentiation based on their density. A large number of adipocytes can be detected, and their density and size can be measured at the single cell level simultaneously. This protocol allows a fast (equilibrium time: ~10 min) and easy way to detect mature adipocytes with a low density that is not possible with other methodologies. The density-based protocol established here may offer a wide range of applications including drug discovery and tissue engineering. The magnetic platform outlined in this study has great potential to be integrated into smartphones or other handheld platforms for point-of-care testing applications, including pathologic tests relevant to the changes in single cell density, such as sickle cell disease and anemia.[94–97] In accordance with this, our system also has the potential to serve as a diagnostic tool for obesity and obesity-related diseases in remote locations. Although the present system is limited to detection, the platform has the potential to be modified into a separation system based on density by providing a flow of the sample to isolate cell groups levitated at distinct heights for further culture or downstream analysis.

Materials and methods

Experimental setup

A magnetic levitation device composed of a microcapillary channel (1 mm × 1 mm cross-section, 50 mm length, and 0.2 mm wall thickness, Vitrocom) between two N52-grade neodymium magnets (NdFeB) (50 mm length, 5 mm height and 2 mm width, Supermagnete) was constructed to create a magnetic field gradient perpendicular to gravity and thus to levitate cells in the paramagnetic medium, and two parallel mirrors (Thorlabs) were placed at 45° to visualize levitation of cells using an inverted microscope (Olympus IX-83).[67]

Cell culture

D1 ORL UVA (mouse bone marrow stem cells)[98] and 7F2 (mouse osteoblasts)[99] were obtained from ATCC. Cells were grown in a growth medium supplemented with 10% fetal bovine serum (FBS) and 1% penicillin/streptomycin at 5% CO_2 humidified atmosphere at 37 °C. D1 ORL UVA and 7F2 cells were cultured in Dulbecco's modified Eagle's medium (DMEM high glucose, Gibco) and alpha modified essential medium (αMEM), respectively. The growth medium was refreshed every 2–3 days, and the cells were passaged every 4–6 days. For differentiation of the D1 ORL UVA cells into adipocytes, the cells were seeded at the concentration of 1000 cells per well in 24-well plates, and after 48 h, adipogenesis was induced by the differentiation medium that contains 10 nM dexamethasone, 50 mM indomethacin, and 5×10^{-3} mg ml^{-1} insulin for 15 days. Likewise, the 7F2 cells were induced in αMEM with induction agents for 10 days. The adipogenic induction medium was replaced every 2–3 days. The cells were imaged at 10× under an inverted microscope (Olympus IX-83).

Magnetic levitation of polymeric beads

Polymer beads with different densities, 1 g mL^{-1}, 1.02 g mL^{-1} (with size of 10–20 μm) and 1.09 g mL^{-1} (with size of 20–27 μm) (Cospheric LLC., ABD), were levitated in the culture medium containing 25 mM, 50 mM or 100 mM gadolinium (Gd^{3+}) (Gadavist®, Bayer). Levitated beads were visualized at 4× under an inverted microscope (Olympus IX-83) after beads reached the equilibrium position (within ~10 min) in the magnetic levitation platform. The levitation heights of the beads (distance from the upper limit of the bottom magnet) were determined using the ImageJ Fiji software.

Magnetic levitation of the cells

D1 ORL UVA cells that were cultured in the growth and adipogenic induction media were trypsinized at the 1st, 5th, 8th, 12th and 15th days and were centrifuged at 125*g* for 5 min. The pellet was resuspended to 10^5 cells per ml in the culture medium containing the gadolinium (Gd^{3+}) paramagnetic agent. Gd^{3+} is a lanthanide metal and can be cytotoxic due to its similarity to the size of Ca^{2+}, causing competitive inhibition for Ca^{2+} involving biological processes. Cytotoxicity of Gd^{3+} can be suppressed by the utilization of commercially available chelate forms.[100,101] In this study, we used Gadavist with a

nontoxic concentration range (≤100 mM) in accordance with our previous findings.[67] Cells were resuspended with concentrations of 25, 50 and 100 mM. Then, 50 μL samples (5000 cell per capillary) were loaded into the microcapillary channel. The samples were levitated until the cells reached the equilibrium position (~10 min) and imaged under the microscope. Later, levitation images were analyzed using ImageJ Fiji software to determine levitation heights/density and cell size. Similarly, 7F2 cells were trypsinized at the 1st, 5th and 10th days and levitated using 25 mM Gd^{3+} concentration within the levitation system. Then, the same analysis method was applied for measuring levitation heights of cells and cell size.

Live/dead assay

D1 ORL UVA cells were seeded at a concentration of 1×10^3 cells per well into a 24-well plate and cultured for 22 days. Cell viability assay (calcein-AM/propidium iodide, Sigma-Aldrich) was carried out to test the viability of levitated cells. The cells were stained for 15 min and levitated using three different concentrations of Gd^{3+} (25, 50 and 100 mM). Then, they were imaged under the fluorescence microscope (Olympus IX-83).

Fluorescent staining and mixing of D1 ORL UVA and 7F2 cells with different ratios

D1 ORL UVA was cultured with the quiescent medium and trypsinized at the 1st, 5th and 10th days. The cells were suspended at the concentration of 1×10^6 cells per mL in the serum-free DMEM culture medium. Then, they were stained with 5 μM of DiO (green) cell-labeling solution (Vybrant™). After incubation at 37 °C for 20 min, the labeled cell suspensions were centrifuged at 1500 rpm for 5 min and the supernatant was removed. The cells were resuspended in the medium. The washing procedure was repeated two more times. Likewise, 7F2 cells were cultured in the αMEM growth medium and adipogenic induction medium. After trypsinization, the cells were suspended at the same concentration in serum-free culture medium and stained with 5 μM of DiI (red) cell-labeling solution using the same protocol. Labeled cells were mixed at different percentages of, 50%, 25%, 10%, 5% and 1%, levitated in magnetic levitation system and imaged under the fluorescence microscope (Olympus IX-83).

Statistical analysis

In this study, all experiments were repeated at least three times. Data on density and levitation height were presented with the mean and standard deviation (mean ± SD) or with the scatter plots and median with the interquartile range. Student's *t*-test (two-tail) or one-way ANOVA with Tukey's multiple comparisons test was used to determine statistical significance, and $P < 0.05$ was considered as statistically significant. The chi-square test was used to test the associations between observed and expected cell ratios in the magnetic levitation device. Graphs showing levitation height *versus* density of beads at different Gd^{3+} concentrations were plotted, and linear regression over the data was performed to obtain equations providing the density of levitated particles/cells levitated in the magnetic detection system.

Author contributions

E. O., H. C. T. and G. M. conceived and designed the study; O. S. and M. A. performed the experiments; E. Y. performed computational simulations; O. S., M. A. and E. O. analyzed the data; O. S., M. A., E. Y., G. M., H. C. T. and E. O. wrote the manuscript.

Conflicts of interest

The authors declare no competing interests.

Acknowledgements

Financial support from The Scientific and Technological Research Council of Turkey (215S862 – E. O., 116M298 – H. C. T.) and Turkish Academy of Sciences (Young Investigator Award – E. O.) is gratefully acknowledged. We thank Sena Yaman for fabricating the magnetic levitation platform. We are also thankful for the helpful discussions with Ozden Yalcın-Ozuysal, PhD.

References

1 E. D. Rosen and B. M. Spiegelman, *Nature*, 2006, **444**, 847–853.
2 B. A. Schmidt and V. Horsley, *Development*, 2013, **140**, 1517–1527.
3 E. E. Kershaw and J. S. Flier, *J. Clin. Endocrinol. Metab.*, 2004, **89**, 2548–2556.
4 R. S. Ahima and J. S. Flier, *Trends Endocrinol. Metab.*, 2000, **11**, 327–332.
5 J. M. Slade, L. M. Coe, R. A. Meyer and L. R. McCabe, *J. Diabetes Complications*, 2012, **26**, 1–9.
6 T. H. Ambrosi, A. Scialdone, A. Graja, S. Gohlke, A.-M. Jank, C. Bocian, L. Woelk, H. Fan, D. W. Logan and A. Schürmann, *Cell Stem Cell*, 2017, **20**, 771–784.e776.
7 M. A. Bredella, P. K. Fazeli, K. K. Miller, M. Misra, M. Torriani, B. J. Thomas, R. H. Ghomi, C. J. Rosen and A. Klibanski, *J. Clin. Endocrinol. Metab.*, 2009, **94**, 2129–2136.
8 P. K. Fazeli, M. A. Bredella, L. Freedman, B. J. Thomas, A. Breggia, E. Meenaghan, C. J. Rosen and A. Klibanski, *J. Bone Miner. Res.*, 2012, **27**, 1864–1871.
9 S. Verma, J. Rajaratnam, J. Denton, J. Hoyland and R. Byers, *J. Clin. Pathol.*, 2002, **55**, 693–698.
10 H.-Y. Liu, A. T. Wu, C.-Y. Tsai, K.-R. Chou, R. Zeng, M.-F. Wang, W.-C. Chang, S.-M. Hwang, C.-H. Su and W.-P. Deng, *Biomaterials*, 2011, **32**, 6773–6780.

11 A. G. Veldhuis-Vlug and C. J. Rosen, *J. Intern. Med.*, 2018, **283**, 121–139.
12 M. F. Pittenger, A. M. Mackay, S. C. Beck, R. K. Jaiswal, R. Douglas, J. D. Mosca, M. A. Moorman, D. W. Simonetti, S. Craig and D. R. Marshak, *science*, 1999, **284**, 143–147.
13 Q. Chen, P. Shou, C. Zheng, M. Jiang, G. Cao, Q. Yang, J. Cao, N. Xie, T. Velletri and X. Zhang, *Cell Death Differ.*, 2016, **23**, 1128.
14 P. Hardouin, T. Rharass and S. Lucas, *Front. Endocrinol.*, 2016, **7**, 85.
15 O. Karadas, G. Mese and E. Ozcivici, *Appl. Biochem. Biotechnol.*, 2018, 1–13.
16 Y. Masamoto, S. Arai, T. Sato, N. Kubota, I. Takamoto, T. Kadowaki and M. Kurokawa, *Stem Cells*, 2017, **35**, 1835–1848.
17 D. Mattiucci, G. Maurizi, V. Izzi, L. Cenci, M. Ciarlantini, S. Mancini, E. Mensà, R. Pascarella, M. Vivarelli and A. Olivieri, *J. Cell. Physiol.*, 2018, **233**, 1500–1511.
18 B. M. Abdallah, *J. Biomed. Sci.*, 2017, **24**, 11.
19 M. A. Bredella, P. K. Fazeli, K. K. Miller, M. Misra, M. Torriani, B. J. Thomas, R. H. Ghomi, C. J. Rosen and A. Klibanski, *J. Clin. Endocrinol. Metab.*, 2009, **94**, 2129–2136.
20 G. Sabatakos, N. Sims, J. Chen, K. Aoki, M. Kelz, M. Amling, Y. Bouali, K. Mukhopadhyay, K. Ford and E. Nestler, *Nat. Med.*, 2000, **6**, 985.
21 G. Duque and D. Rivas, *J. Bone Miner. Res.*, 2007, **22**, 1603–1611.
22 Y. Luo, G.-L. Chen, N. Hannemann, N. Ipseiz, G. Krönke, T. Bäuerle, L. Munos, S. Wirtz, G. Schett and A. Bozec, *Cell Metab.*, 2015, **22**, 886–894.
23 C. J. Rosen and M. L. Bouxsein, *Nat. Rev. Rheumatol.*, 2006, **2**, 35.
24 O. Baskan, G. Mese and E. Ozcivici, *Proc. Inst. Mech. Eng., Part H*, 2017, **231**, 160–168.
25 E. Ozcivici, Y. K. Luu, C. T. Rubin and S. Judex, *PLoS One*, 2010, **5**, e11178.
26 S. Takeshita, T. Fumoto, Y. Naoe and K. Ikeda, *J. Biol. Chem.*, 2014, **289**(24), 16699–16710.
27 E. Ozcivici, Y. K. Luu, B. Adler, Y.-X. Qin, J. Rubin, S. Judex and C. T. Rubin, *Nat. Rev. Rheumatol.*, 2010, **6**, 50.
28 O. Naveiras, V. Nardi, P. L. Wenzel, P. V. Hauschka, F. Fahey and G. Q. Daley, *Nature*, 2009, **460**, 259.
29 R.-J. Zhu, M.-Q. Wu, Z.-J. Li, Y. Zhang and K.-Y. Liu, *Int. J. Hematol.*, 2013, **97**, 58–72.
30 T. Thomas, F. Gori, S. Khosla, M. D. Jensen, B. Burguera and B. L. Riggs, *Endocrinology*, 1999, **140**, 1630–1638.
31 J. Cornish, K. Callon, U. Bava, C. Lin, D. Naot, B. Hill, A. Grey, N. Broom, D. Myers and G. Nicholson, *J. Endocrinol.*, 2002, **175**, 405–415.
32 E. D. Rosen and O. A. MacDougald, *Nat. Rev. Mol. Cell Biol.*, 2006, **7**, 885–896.
33 L. A. Muir, C. K. Neeley, K. A. Meyer, N. A. Baker, A. M. Brosius, A. R. Washabaugh, O. A. Varban, J. F. Finks, B. F. Zamarron, C. G. Flesher, J. S. Chang, J. B. DelProposto, L. Geletka, G. Martinez-Santibanez, N. Kaciroti, C. N. Lumeng and R. W. O'Rourke, *Obesity*, 2016, **24**, 597–605.
34 J. Jo, O. Gavrilova, S. Pack, W. Jou, S. Mullen, A. E. Sumner, S. W. Cushman and V. Periwal, *PLoS Comput. Biol.*, 2009, **5**, e1000324.
35 W. Fei, X. Du and H. Yang, *Trends Endocrinol. Metab.*, 2011, **22**, 204–210.
36 C. Durandt, F. A. van Vollenstee, C. Dessels, K. Kallmeyer, D. de Villiers, C. Murdoch, M. Potgieter and M. S. Pepper, *J. Lipid Res.*, 2016, **57**, 729–742.
37 Y. Guo, T. C. Walther, M. Rao, N. Stuurman, G. Goshima, K. Terayama, J. S. Wong, R. D. Vale, P. Walter and R. V. Farese, *Nature*, 2008, **453**, 657.
38 P. Greenspan, E. P. Mayer and S. D. Fowler, *J. Cell Biol.*, 1985, **100**, 965–973.
39 J. Ramirez-Zacarias, F. Castro-Munozledo and W. Kuri-Harcuch, *Histochemistry*, 1992, **97**, 493–497.
40 X. Xia, W. Chen, T. Ma, G. Xu, H. Liu, C. Liang, X. Bai, Y. Zhang, Y. He and T. Liang, *Liver Transplant.*, 2012, **18**, 696–706.
41 M. De Sousa, D. P. Porras, C. G. Perry, P. Seale and A. Scimè, *Stem Cells*, 2014, **32**, 1323–1336.
42 A.-A. Ghoniem, Y. Açil, J. Wiltfang and M. Gierloff, *Anat. Cell Biol.*, 2015, **48**, 85–94.
43 T. Fink, L. Abildtrup, K. Fogd, B. M. Abdallah, M. Kassem, P. Ebbesen and V. Zachar, *Stem Cells*, 2004, **22**, 1346–1355.
44 B. B. Boumelhem, S. J. Assinder, K. S. Bell-Anderson and S. T. Fraser, *Adipocyte*, 2017, **6**, 112–123.
45 S. M. Majka, H. L. Miller, K. M. Helm, A. S. Acosta, C. R. Childs, R. Kong and D. J. Klemm, *Methods Enzymol.*, 2014, **537**, 281–296.
46 R. Bernstein, W. C. Hyun, J. H. Davis, M. J. Fulwyler and H. A. Pershadsingh, *Cytometry*, 1989, **10**, 469–474.
47 K. Thelen, N. Ayala-Lopez, S. W. Watts and G. A. Contreras, *J. Visualized Exp.*, 2017, (124), e55818.
48 C. Hepler, L. Vishvanath and R. K. Gupta, *Genes Dev.*, 2017, **31**, 127–140.
49 F. Liu, K. Pawan, G. Zhang and J. Zhe, *PLoS One*, 2017, **12**, e0172697.
50 N. Norouzi, H. C. Bhakta and W. H. Grover, *PLoS One*, 2017, **12**, e0180520.
51 P. O. Bagnaninchi and N. Drummond, *Proc. Natl. Acad. Sci. U. S. A.*, 2011, 201018260.
52 J. P. Smus, C. C. Moura, E. McMorrow, R. S. Tare, R. O. Oreffo and S. Mahajan, *Chem. Sci.*, 2015, **6**, 7089–7096.
53 C. Steuwe, I. I. Patel, M. Ul-Hasan, A. Schreiner, J. Boren, K. M. Brindle, S. Reichelt and S. Mahajan, *J. Biophotonics*, 2014, **7**, 906–913.
54 A. Wyllie and R. Morris, *Am. J. Pathol.*, 1982, **109**, 78.
55 A. A. Kumar, M. R. Patton, J. W. Hennek, S. Y. Lee, G. D'Alesio-Spina, X. Yang, J. Kanter, S. S. Shevkoplyas, C. Brugnara and G. M. Whitesides, *Proc. Natl. Acad. Sci. U. S. A.*, 2014, **111**, 14864–14869.
56 A. K. Bryan, A. Goranov, A. Amon and S. R. Manalis, *Proc. Natl. Acad. Sci. U. S. A.*, 2010, **107**(3), 999–1004.

57 C. F. Kurat, H. Wolinski, J. Petschnigg, S. Kaluarachchi, B. Andrews, K. Natter and S. D. Kohlwein, *Mol. Cell*, 2009, **33**, 53–63.
58 W. H. Grover, A. K. Bryan, M. Diez-Silva, S. Suresh, J. M. Higgins and S. R. Manalis, *Proc. Natl. Acad. Sci. U. S. A.*, 2011, **108**, 10992–10996.
59 A. K. Bryan, V. C. Hecht, W. Shen, K. Payer, W. H. Grover and S. R. Manalis, *Lab Chip*, 2014, **14**, 569–576.
60 P. Björntorp, M. Karlsson, H. Pertoft, P. Pettersson, L. Sjöström and U. Smith, *J. Lipid Res.*, 1978, **19**, 316–324.
61 M. Fernyhough, J. Vierck, G. Hausman, P. Mir, E. Okine and M. Dodson, *Cytotechnology*, 2004, **46**, 163–172.
62 N. G. Durmus, H. C. Tekin, S. Guven, K. Sridhar, A. Arslan Yildiz, G. Calibasi, I. Ghiran, R. W. Davis, L. M. Steinmetz and U. Demirci, *Proc. Natl. Acad. Sci. U. S. A.*, 2015, **112**, E3661–E3668.
63 Y. Zhao, H. S. S. Lai, G. Zhang, G.-B. Lee and W. J. Li, *Lab Chip*, 2014, **14**, 4426–4434.
64 N. Cermak, S. Olcum, F. F. Delgado, S. C. Wasserman, K. R. Payer, M. A. Murakami, S. M. Knudsen, R. J. Kimmerling, M. M. Stevens and Y. Kikuchi, *Nat. Biotechnol.*, 2016, **34**, 1052.
65 S. Tasoglu, J. A. Khoory, H. C. Tekin, C. Thomas, A. E. Karnoub, I. C. Ghiran and U. Demirci, *Adv. Mater.*, 2015, **27**, 3901–3908.
66 S. Yaman, M. Anil-Inevi, E. Ozcivici and H. C. Tekin, *Front. Bioeng. Biotechnol.*, 2018, **6**, 192.
67 M. Anil-Inevi, S. Yaman, A. A. Yildiz, G. Mese, O. Yalcin-Ozuysal, H. C. Tekin and E. Ozcivici, *Sci. Rep.*, 2018, **8**, 7239.
68 M. V. Berry and A. K. Geim, *Eur. J. Phys.*, 1997, **18**, 307.
69 K. A. Mirica, S. S. Shevkoplyas, S. T. Phillips, M. Gupta and G. M. Whitesides, *J. Am. Chem. Soc.*, 2009, **131**, 10049–10058.
70 J. Xie, P. Zhao, Z. Jing, C. Zhang, N. Xia and J. Fu, *J. Magn. Magn. Mater.*, 2018, **468**, 100–104.
71 S. Ge, Y. Wang, N. J. Deshler, D. J. Preston and G. M. Whitesides, *J. Am. Chem. Soc.*, 2018, **140**(24), 7510–7518.
72 S. Ge and G. M. Whitesides, *Anal. Chem.*, 2018, **90**(20), 12239–12245.
73 C. Zhang, P. Zhao, F. Gu, J. Xie, N. Xia, Y. He and J. Fu, *Anal. Chem.*, 2018, **90**, 9226–9233.
74 Q.-H. Gao, W.-B. Li, H.-X. Zou, H. Yan, Z.-K. Peng, G. Meng and W.-M. Zhang, *Sens. Actuators, B*, 2019, **287**, 64–70.
75 S. M. Knudsen, M. G. von Muhlen, D. B. Schauer and S. R. Manalis, *Anal. Chem.*, 2009, **81**, 7087–7090.
76 T. A. Juopperi, W. Schuler, X. Yuan, M. I. Collector, C. V. Dang and S. J. Sharkis, *Exp. Hematol.*, 2007, **35**, 335–341.
77 W. H. Bloxham, J. W. Hennek, A. A. Kumar and G. M. Whitesides, *Anal. Chem.*, 2015, **87**, 7485–7491.
78 A. Martin, M. Daniel, D. Drinkwater and J. Clarys, *Int. J. Obes. Relat. Metab. Disord.*, 1994, **18**, 79–83.
79 Y. Zhao, H. S. Lai, G. Zhang, G. B. Lee and W. J. Li, *Biomicrofluidics*, 2015, **9**, 022406.
80 J. Knittle, K. Timmers, F. Ginsberg-Fellner, R. Brown and D. Katz, *J. Clin. Invest.*, 1979, **63**, 239–246.
81 M. Krotkiewski, P. Björntorp, L. Sjöström and U. Smith, *J. Clin. Invest.*, 1983, **72**, 1150–1162.
82 Y. D. Tchoukalova, C. Koutsari, M. V. Karpyak, S. B. Votruba, E. Wendland and M. D. Jensen, *Am. J. Clin. Nutr.*, 2008, **87**, 56–63.
83 P. E. Fielding and C. J. Fielding, in *New Comprehensive Biochemistry*, Elsevier, 2002, vol. 36, pp. 527–552.
84 T. C. Walther and R. V. Farese Jr., *Annu. Rev. Biochem.*, 2012, **81**, 687–714.
85 L.-H. Loo, H.-J. Lin, D. K. Singh, K. M. Lyons, S. J. Altschuler and L. F. Wu, *J. Cell Biol.*, 2009, **187**, 375–384.
86 T. T. Le and J.-X. Cheng, *PLoS One*, 2009, **4**, e5189.
87 Y.-H. Lee, S.-Y. Chen, R. J. Wiesner and Y.-F. Huang, *J. Lipid Res.*, 2004, **45**, 1162–1167.
88 T. Björnheden, B. Jakubowicz, M. Levin, B. Odén, S. Edén, L. Sjöström and M. Lönn, *Obes. Res.*, 2004, **12**, 95–105.
89 T. Skurk, C. Alberti-Huber, C. Herder and H. Hauner, *J. Clin. Endocrinol. Metab.*, 2007, **92**, 1023–1033.
90 J. I. Kim, J. Y. Huh, J. H. Sohn, S. S. Choe, Y. S. Lee, C. Y. Lim, A. Jo, S. B. Park, W. Han and J. B. Kim, *Mol. Cell. Biol.*, 2015, **35**, 1686–1699.
91 H. C. Chen and R. V. Farese, *J. Lipid Res.*, 2002, **43**, 986–989.
92 H. E. Kubitschek, *CRC Crit. Rev. Microbiol.*, 1987, **14**, 73–97.
93 W. W. Baldwin, R. Myer, N. Powell, E. Anderson and A. L. Koch, *Arch. Microbiol.*, 1995, **164**, 155–157.
94 S. Knowlton, I. Sencan, Y. Aytar, J. Khoory, M. Heeney, I. Ghiran and S. Tasoglu, *Sci. Rep.*, 2015, **5**, 15022.
95 B. Yenilmez, S. Knowlton, C. H. Yu, M. M. Heeney and S. Tasoglu, *Adv. Mater. Technol.*, 2016, **1**, 1600100.
96 B. Yenilmez, S. Knowlton and S. Tasoglu, *Adv. Mater. Technol.*, 2016, **1**, 1600144.
97 E. J. Felton, A. Velasquez, S. Lu, R. O. Murphy, A. ElKhal, O. Mazor, P. Gorelik, A. Sharda and I. C. Ghiran, *Lab Chip*, 2016, **16**, 3286–3295.
98 L. Demiray and E. Özçivici, *Turk. J. Biol.*, 2015, **39**, 88–97.
99 S. Muruganandan, A. A. Roman and C. J. Sinal, *J. Bone Miner. Res.*, 2010, **25**, 222–234.
100 M. Rogosnitzky and S. Branch, *BioMetals*, 2016, **29**, 365–376.
101 A. D. Sherry, P. Caravan and R. E. Lenkinski, *J. Magn. Reson. Imaging*, 2009, **30**, 1240–1248.